Imaging Buried Interfacial Lattices with Quantized Electrons

I. B. Altfeder and D. M. Chen
The Rowland Institute for Science, Cambridge, Massachusetts 02142

K. A. Matveev
Department of Physics, Duke University, Durham, North Carolina 27708
(Received 16 October 1997)

We demonstrate that the well-known Si(111)-(7 × 7) superlattice buried under as much as 100 Å of crystalline Pb can be directly imaged with a scanning tunneling microscope at 77 K. The unexpected transparency of the metal and the high lateral resolution are the result of a nondiffractive scattering of the electrons at the interface. We attribute this phenomenon to a large anisotropy of the effective masses associated with the free in-plane and the quantized transverse motion of the electrons. [S0031-9007(98)06246-2]

PACS numbers: 61.16.Ch, 71.18.+y, 73.20.Dx, 79.60.Jv

Buried interfacial structure is the building foundation upon which rests a desired material in any heteroepitaxy system. Probing the interfacial structure and its evolution during the growth is essential to our understanding and to the ability to ultimately control the morphology and physical properties of the epitaxial film. Despite the rapid advancement in many microscopy fields in recent decades, *in situ* and *nondestructive* determination of a buried interfacial structure *to an atomic scale* remains a formidable task. The difficulty stems from a weak signal involving only one or two atomic layers on the one hand, and significant attenuation or dephasing of the probing waves as they traverse the burying layers on the other. Traditionally, much of the buried interface analysis is accomplished with *destructive* techniques such as cross-sectional TEM. But in recent years, significant progress has been made in a number of nondestructive approaches. With the help of the intense synchrotron light source, grazing-incidence x-ray diffraction, and soft x-ray spectroscopy have been used for characterizing the interfacial reconstruction and chemical composition [1]. Low energy electron microscopy has been used to observe both atomic steps and dislocations at the Si/Ag interface [2]. Ion-implantation-induced subsurface noble gas bubbles have been revealed by scanning tunneling microscopy (STM) [3]. Interfacial point defects are identified by ballistic electron emission microscopy [4].

In this Letter, we report our successful attempt to directly image the well-known Si(111)-(7 × 7) superstructure [5] buried under as much as 100 Å of Pb using a low temperature STM operating at 77 K. The ability to probe a buried interface morphology with STM has been clearly demonstrated in our previous Letter [6]. It has been shown that the buried atomic terraces manifest themselves through interference fringes while the absolute depth is unveiled in the quantum states (QS) energy spectra [7,8]. Thus, a simple one-dimensional quantization for the first time makes possible *in situ* nondestructive characterization of the metal overlayers grown on a semiconductor *in all three dimensions.* In our experiments, we exploit the fact that, through the matching of the boundary conditions, the wave function of an electron under confinement in the metal region should contain the imprints of both the vacuum and buried interfaces. Thus the internal quantized electrons are an ideal probe of the buried interface, which in some ways is superior to an external source. The question remains: What is the fundamental limit of the lateral resolution given the fact that the two-dimensional (2D) in-plane motion of electrons remains free? Consider the normal incident electrons scattered off an interfacial feature of a lateral size σ; the Heisenberg uncertainty principle should lead to the angular divergence of the scattered electrons $\sim\alpha(\lambda/\sigma)$, where λ is the electron de Broglie wavelength, and $\alpha = m_\perp/m_\parallel$ is the ratio of the effective masses of the electron normal and parallel to the film. As a result, at the opposite side of the film the feature is projected with the size of $\sigma + H\alpha(\lambda/\sigma)$, H being the thickness of the film. Thus, the best lateral resolution is estimated to be $\sigma \sim (\alpha H\lambda)^{1/2}$. For a free electron gas ($\alpha = 1$) to resolve the interface feature with a size on the order of the Fermi wavelength λ_F, its thickness should be of the same order. Thus, achieving atomic resolution for a lattice buried under a thickness of practical interest seems not permissible. But, as we shall show below, owing to the unique topology of the Fermi surface (FS) in metals, the ratio of the effective masses α can be significantly reduced. Together with the strong quantization, this results in the nondiffractive scattering and, hence, in a great enhancement of the resolving power.

To explore the attainable lateral resolution, we choose the well-known Si(111)-(7 × 7) reconstruction as the substrate on which we deposited Pb while keeping the substrate below room temperature. Previous studies have shown that, under such preparation procedures, the underlying Si(111)-(7 × 7) remains intact and the Pb forms (111) crystallites following the initial growth of two wetting layers [9,10].

Our experiment was performed in a 5×10^{-11} Torr ultrahigh vacuum chamber which integrates a homemade low temperature STM operational from room temperature down to 5 K with a sample fabrication chamber equipped with an Auger spectrometer, a reflection high-energy electron diffraction (RHEED) system, and a number of molecular-beam epitaxy cells. The Si(111)-(7 × 7) substrate is prepared using a routine sputtering and annealing procedure. Pb atoms are deposited on the clean surface from an effusion cell held at 500 °C at a rate of ~1 ML/min. Both RHEED and Auger spectrometers were used to verify and control the specimen preparation. STM images were acquired at 77 K in the constant current mode. The images obtained on top of the Pb overlayers are calibrated against images of a clean Si(111)-(7 × 7) taken at the same temperature.

A large number of Pb islands have been studied in our experiment. Their lateral dimension ranges from 500 to 3000 Å, and the corresponding height varies from 12 to 100 Å. A typical STM image of the Pb crystallites on the Si(111)-(7 × 7) surface is similar to that shown in our previous Letter [6]. The top of a Pb island is atomically flat even when it expands many terraces of the substrate, except for a small lattice mismatch between adjacent terraces. Under appropriate bias conditions, STM can detect the interference patterns of the quantized electrons with those in an odd number of Pb layers giving rise to bright fringes and the ones in an even number of layers dark fringes, or vice versa. These binary fringes result from the simple fact that the spacing between two (111) planes of Pb $d_0 \approx \lambda_F/4$.

Higher resolution STM images reveal that within each fringe there exists a fine structure. Figure 1(a) is a typical image taken with a tip bias of −0.5 V over a bright fringe. It exhibits a hexagonal lattice with a period of 27 Å. Both the size and the axes of symmetry of the superlattice coincide with that of the Si(111)-(7 × 7) reconstruction of the substrate. The variation of the intensity in Fig. 1(a) is caused by a weaker modulation of a period of ~81 Å along the same orientation, as can be better seen in the Fourier transform of Fig. 1(c), as well as in the zoom-out of Fig. 1(b).

STM images similar to Figs. 1(a) and 1(b) can be observed with a range of tip bias from −0.6 to −0.4 V. When the tip bias is reduced further to −0.3 V, however, there is an abrupt change of the image contrast but not the period, as shown in Fig. 2(a). This change is accompanied by a switching of the fringe contrast from bright to dark. Figure 2(b) is an image of the same region acquired at −0.5 V tip bias. Thus, these two types of images appear to be a pair of complementary pictures, and we shall refer to them as *positive* [Fig. 2(b)] and *negative* [Fig. 2(a)], respectively.

The switching between positive and negative images depends not only on the tip bias but also on the thickness of Pb. For a given bias, this occurs when the number of Pb layers is changed by one and the corresponding fringe is flipped. An example of this is shown in Fig. 2(c). Keep in mind that the surface of this image is atomically flat and the step diagonally across the image reflects the change of fringe contrast as a result of an underlying atomic step. *Thus positive and negative images are always associated, respectively, with bright and dark fringes.*

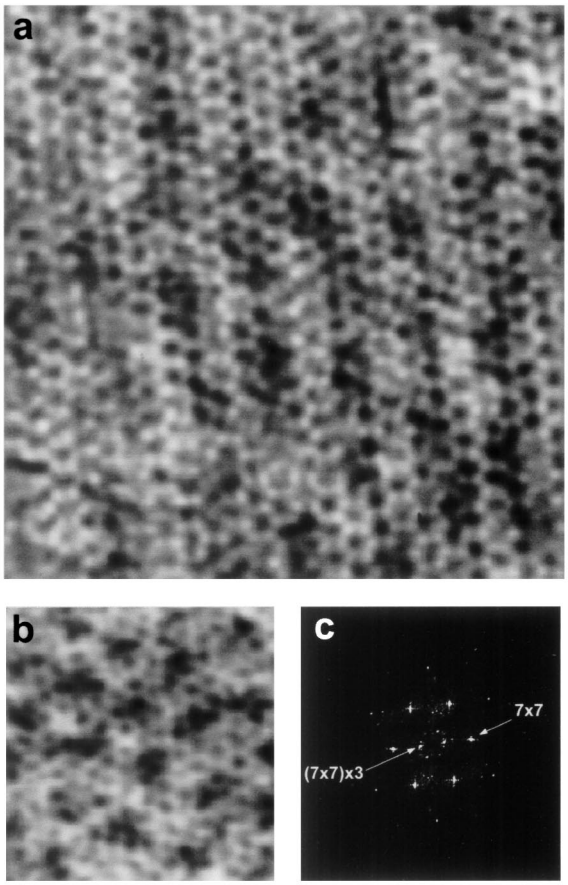

FIG. 1. (a) A 550 × 550 Å STM image of a superlattice within a bright interference fringe acquired on a 60 Å thick Pb crystallite with a tip bias of −0.5 V. Both the size of the unit cell (27 Å) and the principal axes of the superlattice coincide with that of the Si(111)-(7 × 7) reconstruction of the substrate, but the intensity is modulated with a longer period of ~81 Å. (b) 330 × 330 Å STM image showing the ×3 spatial modulation of the superlattice. (c) Fourier transfer of the superlattice image showing both spatial frequencies.

The internal fine structure of a fringe is intimately connected with the local variation of the energy spectra of the electron confined in the thin Pb film, as revealed by our site-specific *I-V* measurements. Figure 3 shows two distinct *I-V* characteristics that are obtained over both even (curves 1) and odd (curves 2) numbers of Pb layers. Curves 1a and 2a acquired at site *A* (see inset of Fig. 3) display a staircaselike tunnel spectrum similar to those reported previously [6]. It has been shown that the energy separation Δ between QS near the Fermi level equals $\pi\hbar v_F/H$, v_F being the Fermi velocity; and the energy shift δ between two such corresponding QS for N and

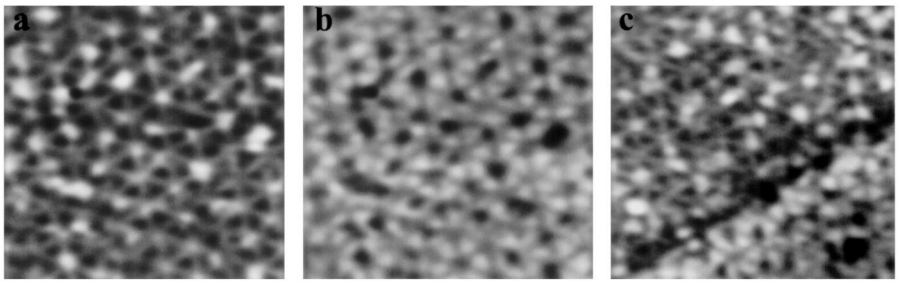

FIG. 2. (a) A 240 × 240 Å STM image of a similar superlattice as Fig. 1 acquired over a dark fringe with a tip bias reduced down to −0.3 V. (b) A STM image of the same region as (a) taken at −0.5 V bias. (c) A 270 × 270 Å STM image showing the superlattices on both the dark and the bright (lower right) fringes that are complementary images like (a), a negative, and (b), a positive. The diagonal boundary is caused by the underlying atomic step of the Si substrate.

$N + 1$ Pb layers is $2d_0\Delta/\lambda_F$, or roughly $\Delta/2$ for Pb. These current steps are smeared out when the spectra are collected at site *B* (curves 1b and 2b) and site *C* (spectra not shown). These *I*-*V* characteristics offer an empirical explanation for the abrupt contrast switching behavior. For a given Pb thickness (curves 1a and 1b, for example) at −0.3 V, tip bias conductance at site *A* is higher than that at site *B*, while at −0.5 V, the opposite is true and the switching occurs at −0.4 V for this particular case. For a fixed bias of −0.5 V, on the other hand, the conductance at site *A* is higher than that at site *B* for the odd number of layers of Pb, but the opposite holds for the even number of layers. Furthermore, it is evident that when the tip bias is set near a step of the *I*-*V* spectrum, the contrast of the fine structure is optimized, as experienced in our measurements.

Collectively, the above observations suggest that the internal fine structure of the fringe is originated from the buried interface, rather than the top surface of the Pb. Indeed, when we substitute the Si(111)-(7 × 7) with a Si(100) substrate on which Pb is known to grow (111) crystallites as well [11], we observed lattices of only twofold symmetry associated with the dimerized surface of Si(100) [12]. We therefore conclude that this fine structure is an image of the buried (7 × 7) Pb/Si(111) interfacial lattice, the vortices being the corner holes and border lines being the dimer chains as depicted in the inset of Fig. 3.

Although the Si(111)-(7 × 7) reconstruction remains intact under a Pb film, the adatoms are most likely displaced by Pb atoms, forming an alloyed layer. We speculate that patches of Si atoms are responsible for the imaged defect (white protrusions) visible in Fig. 2(a). Notice that the lattice parameters for the (111) plane of Si and Pb are $a_{\mathrm{Si}} = 3.84$ Å and $a_{\mathrm{Pb}} = 3.51$ Å, respectively. A superlattice commensurate with both of these two lattices should contain 21 Si units or 23 Pb units, and, hence, have a period of 80.7 Å. Within the measurement accuracy, this lattice coincides with the 3 times modulation of the (7 × 7) lattice of Figs. 1(a)–1(c), and, hence, is presumed to be the cause of the latter. This conjecture implies that the Pb lattice manifests itself through a beating with the Si lattice in the STM images.

Quite surprisingly, the buried (7 × 7) interfacial atomic lattice can be imaged under as much as 100 Å of Pb with only a very small degradation of the contrast and sharpness of the detailed features. According to the resolution argument given earlier, this could only be possible if $\alpha \ll 1$.

To gain a theoretical insight into the enhanced lateral resolution, let us examine the tunneling density of states $\nu(E, \rho)$ as a function of electron energy E and tip position

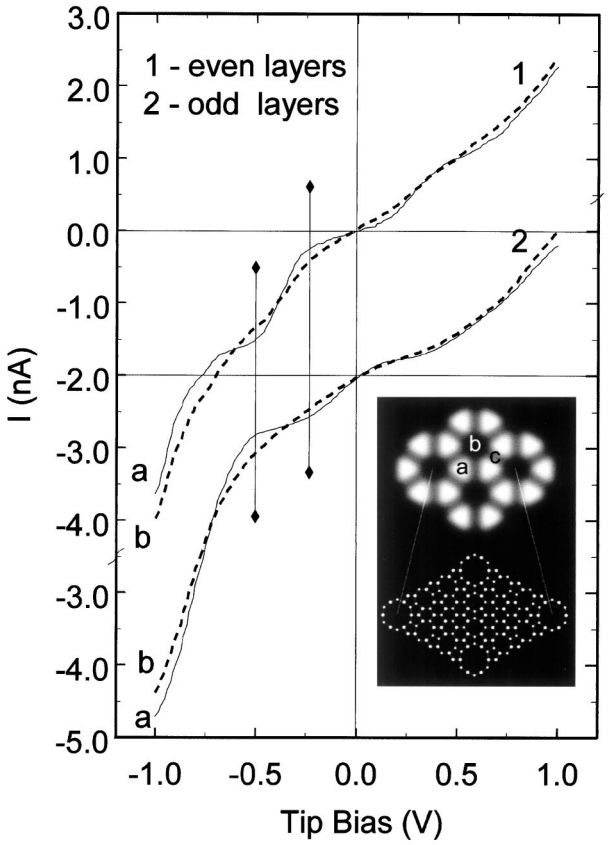

FIG. 3. Site-specific *I*-*V* spectra taken over regions of odd and even numbers of Pb layers, respectively. Inset shows an idealized positive image of the superlattice and the corresponding Si(111)-(7 × 7) lattice under burial with adatoms being removed. The letters mark the three distinct sites on which *I*-*V* measurements are performed.

$\rho = (x, y)$ at the surface of the Pb film, $z = H$. The density of states ν is proportional to the imaginary part of the electron Green's function $G_E(\boldsymbol{r}, \boldsymbol{r})$, which in the case of a film with smooth boundaries can be written in the form

$$G_E^0(\boldsymbol{r}, \boldsymbol{r}') = \sum_n \varphi_n(z)\varphi_n(z') g_n(\boldsymbol{r} - \boldsymbol{r}', E),$$
$$g_n(\boldsymbol{r}, E) = \int \frac{d\boldsymbol{k}}{(2\pi)^2} \frac{e^{i\boldsymbol{k}\boldsymbol{r}}}{E - E_n - \varepsilon_{n\boldsymbol{k}} + i\delta}. \quad (1)$$

Here E_n and $\varphi_n(z)$ are subband energies and wave functions, respectively, and $\varepsilon_{n\boldsymbol{k}}$ is the energy of the nth subband of in-plane motion of electrons with a wave vector of $\boldsymbol{k} = (k_x, k_y)$.

To account for the interface roughness we add a small-size defect modeled by a potential $V(\boldsymbol{r}) = \boldsymbol{v}\delta(\boldsymbol{r})$. The presence of the defect modifies the Green's function, and at $\boldsymbol{v} \to \infty$ one easily finds

$$G_E(\boldsymbol{r}, \boldsymbol{r}) = G_E^0(\boldsymbol{r}, \boldsymbol{r}) - \frac{G_E^0(\boldsymbol{r}, \boldsymbol{0}) G_E^0(\boldsymbol{0}, \boldsymbol{r})}{G_E^0(\boldsymbol{0}, \boldsymbol{0})}. \quad (2)$$

The pronounced steps in the I-V curves such as those of Fig. 3 indicate that the density of states has sharp peaks near the subband energies E_n. This means that the dominant contribution to the density of states near step position is due to only one term in Eq. (1). Thus, at E close to E_n we can substitute $G_E^0(\boldsymbol{r}, \boldsymbol{r}') \approx \varphi_n(z)\varphi_n(z') g_n(\rho - \rho', E)$ into Eq. (1), and find

$$G_E(\boldsymbol{r}, \boldsymbol{r}) \approx [\varphi_n(H)]^2 \left[g_n(\boldsymbol{0}, E) - \frac{g_n(\rho, E) g_n(-\rho, E)}{g_n(\boldsymbol{0}, E)} \right]. \quad (3)$$

Equation (3) shows that when the STM tip is positioned over a strong impurity, $\rho = \boldsymbol{0}$, the peak in the density of states, given by the imaginary part, disappears. This suppression of the peak in the density of states is clearly seen in our data as a smearing of the steps in the tunnel I-V curve on Fig. 3. At large distances from the impurity, $\rho \to \infty$, the two-dimensional Green's function $g_n(\rho, E)$ vanishes, and the peak in the density of states is restored.

The typical size a of a region around the impurity where the density of states is suppressed is determined by the ρ dependence of $g_n(\rho, E)$. It follows from the definition in Eq. (1) that

$$a \sim \pi/|\boldsymbol{k}|, \quad (4)$$

where $\boldsymbol{k}$ is such that $\varepsilon_{n\boldsymbol{k}} = E - E_n$. For example, if the in-plane electron spectrum is quadratic, $\varepsilon_{n\boldsymbol{k}} = \hbar^2 k^2 / 2m_\parallel$, we have $k = \sqrt{2m_\parallel(E - E_n)}/\hbar$, and $g_n(\rho, E) = (im_\parallel/2\hbar^2) H_0^{(1)}(k\rho)$, where $H_0^{(1)}$ is the Hankel function. It then follows from Eq. (3) that

$$a \sim \hbar/\sqrt{2m_\parallel(E - E_n)}. \quad (5)$$

Equation (5) diverges as $E \to E_n$, implying a total loss of resolution. In the experiment, this is precisely the situation when the two I-V curves cross each other at the step (Fig. 3). Since $E - E_n \le \Delta/2$, Eq. (5) predicts that the smallest attainable feature size $a \sim \hbar/\sqrt{m_\parallel \Delta}$, and when substituting Δ with $\pi\hbar v_F/H$, it gives the similar estimate of the resolution as obtained from the uncertainty principle argument. Thus, a larger Δ and a smaller α are essential to a good lateral resolution. We note that, near the [111] symmetry point, the hole FS of Pb is nearly flat [13] which, indeed, gives rise to a large in-plane effective mass. For larger $|\boldsymbol{k}|$, however, the FS strongly deviates from a Fermi sphere and the quadratic spectrum is not applicable. In this regime, $|\boldsymbol{k}|$, determined from the (111) sections of the FS, is nearly constant and $\sim k_F$. Thus from Eq. (4) we have $a \sim \lambda_F/2$. This explains well why the experimentally attained resolution ($\approx$6 Å) does not change appreciably for samples of various heights.

In conclusion, we have shown that an interfacial lattice buried under a film of Pb whose thickness is as many as 10 times the Fermi wavelength can be clearly imaged with STM. The key to the transparency of a metal and such an excellent lateral resolution lies in a highly anisotropic motion of the electrons and the strong quantization of their transverse components. Since a great number of materials exhibit various degrees of anisotropy of the effective masses, we expect our present finding to be applicable in many other heteroepitaxy systems. Undoubtedly, detecting the evolution of the interface structure as a result of material deposition or thermal treatment will be one of the most valuable applications of this technique in future work.

We thank J. Fournier and J. Parks for valuable discussions. This work was supported by The Rowland Institute for Science.

[1] D. L. Ederer *et al.*, J. Vac. Sci. Technol. A **14**, 859 (1996).
[2] R. M. Tromp *et al.*, Phys. Rev. Lett. **71**, 3299 (1993).
[3] M. Schmid *et al.*, Phys. Rev. Lett. **76**, 2298 (1996).
[4] T. Meyer and H. v. Kanel, Phys. Rev. Lett. **78**, 3133 (1997).
[5] K. Takayanagi *et al.*, J. Vac. Sci. Technol. A **3**, 1502 (1985).
[6] I. B. Altfeder, K. A. Matveev, and D. M. Chen, Phys. Rev. Lett. **78**, 2815 (1997).
[7] R. C. Jaklevic *et al.*, Phys. Rev. Lett. **26**, 88 (1971).
[8] M. Jalochowski *et al.*, Phys. Rev. B **46**, 4693 (1992).
[9] H. H. Weitering, D. R. Heslinga, and T. Hibma, Phys. Rev. B **45**, 5991 (1992).
[10] F. Gray *et al.*, J. Phys. (Paris) **50**, 7181 (1989).
[11] L. Li *et al.*, Phys. Rev. B **50**, 10 834 (1994).
[12] I. B. Altfeder and D. M. Chen (to be published).
[13] J. R. Anderson and A. V. Gold, Phys. Rev. **139**, A1459 (1965).